Nanoscale electron-beam-stimulated processing

P. D. Rack, S. Randolph, Y. Deng, J. Fowlkes, Y. Choi, and D. C. Joy

Citation: Applied Physics Letters **82**, 2326 (2003); doi: 10.1063/1.1565696
View online: http://dx.doi.org/10.1063/1.1565696
View Table of Contents: http://scitation.aip.org/content/aip/journal/apl/82/14?ver=pdfcov
Published by the AIP Publishing

Nanoscale electron-beam-stimulated processing

P. D. Rack,[a] S. Randolph, Y. Deng, J. Fowlkes, Y. Choi, and D. C. Joy
Department of Materials Science and Engineering, The University of Tennessee, Knoxville, Tennessee 37996-2200

(Received 27 December 2002; accepted 10 February 2003)

Electron-beam-stimulated deposition and etching has been investigated as a clean, alternative method for nanoscale selective processing. Depositions using $W(CO)_6$ and hydrocarbon sources have yielded efficient and selective electron-beam deposits. Primarily fluorine-based precursors have been used to etch a variety of materials. Initial results regarding the selective etching of silicon and silicon dioxide suggest that inelastic scattering of the primary electron beam with the gas occurs and is more severe at lower beam energies. The etch rate increases linearly with decreasing electron-beam energy, however, it is not clear if this is due to enhanced primary- or secondary-electron-stimulated processes. Feature sizes as small as 55 nm have been selectively processed. © *2003 American Institute of Physics.* [DOI: 10.1063/1.1565696]

The ability to manipulate materials at the nanoscale is critical for the nanotechnology revolution that is occurring. The intelligent design, fabrication, and repair of nanoscale devices require techniques to selectively and nanoscopically deposit and remove material in a controllable fashion. Current technologies to selectively deposit or etch microscopic features utilize ion-beam deposition and etching, laser ablative etching using far-field and near-field optics, and mechanical abrasion using a fine microtip. Of these techniques, focused-ion-beam techniques are probably the most mature technology that has been extended to application at the nanoscale. When using an ion beam to stimulate a deposition or etch process, the gallium ions get implanted into the substrate, which can significantly change the optical, electrical, or mechanical properties of the substrate. Charging inherent to the ion–solid interaction also causes proximity effects and can also lead to so-called ''riverbed effects,'' which erode nearby features when the heavy ion beam is scattered and induces sputtering.

Electron-beam-stimulated deposition and etching is conceptually similar to the existing focused-ion-beam approach and has been shown to be a viable technique for depositing nanoscopic materials. A variety of materials have been deposited using a focused electron beam including carbon,[1] chromium,[2] gold,[3–5] iron,[6–7] silicon,[8] silicon oxide,[9] palladium,[10] platinum,[11,12] and tungsten.[13–21] Fewer investigators have explored electron-beam etching, however, photoresist,[22,23] silicon,[24,25] silicon dioxide,[24] silicon nitride,[24] and tantalum/tantalum nitride[25] have been reported.

The main advantage of using an electron beam rather than an ion beam is reduced contamination. The deleterious optical, electrical, and mechanical properties that implanted gallium ions can induce are obviated when using an electron beam, which is commonly used nondestructively when imaging in a scanning electron microscope (SEM). Another potential advantage of electron-stimulated processes over ion-beam techniques is the reduced charging effect that can result in better spatial control of the electron beam. For example, by operating at the ''crossover'' energy, where the sum of the secondary and backscattered electron emission coefficients equals unity, can significantly reduce charging. In addition, if a low-pressure gas flux is directed onto a surface irradiated by an electron beam, then the production of positive ions results, effectively neutralizing the buildup of negative charge.

To explore the electron-beam-stimulated process, a gas delivery system was designed and attached to a Hitachi S-3500N variable pressure (SEM) (VPSEM). The VPSEM has a tungsten hairpin source and is equipped with a backscatter detector, an energy dispersive x-ray spectrometer (EDS), and has a pump system designed to operate in high vacuum or variable pressure mode (up to 0.1–300 Pa). The gas delivery system was designed to deliver up to four gases to a hypodermic needle for localized gas injection. The injection system is mounted on a wobble stick for three-dimensional positioning capability.

To date, most of the deposition efforts have focused on selective tungsten (W) deposition using a tungsten hexacarbonyl $[W(CO)_6]$ source. $W(CO)_6$ is a solid state source at room temperature and pressure. To deliver the $W(CO)_6$ gas, the solid source is heated to $45-80\,^{\circ}C$, which raises the vapor pressure enough to deliver ~ 0.1 Pa of gas into the SEM. EDS measurements were taken *in situ* to temporally monitor the deposition process and after the deposition was completed to quantify the final film deposit. Germanium, as opposed to silicon, was used as the substrate material because Si and W have overlapping EDS peak signatures making it difficult to determine the composition of the deposit. Figure 1 shows some initial results of deposition using a $W(CO)_6$ source. A series of $2.5\ \mu m \times 2.5\ \mu m$ tungsten boxes were deposited over a range of times from 5–30 min in 5 min increments using a 5 keV beam energy. Figure 1(b) is a SEM micrograph of the six deposits showing the gradual thickening of deposits with increasing $W(CO)_6$ exposure and (a) is the EDS spectra acquired using a probe beam energy of 5 keV, after each run, which shows the germanium substrate signal decreasing and the W, C, and O peaks increasing with increasing time. Figure 2 shows an array of ~ 55 and 85 nm

[a]Electronic mail: prack@utk.edu

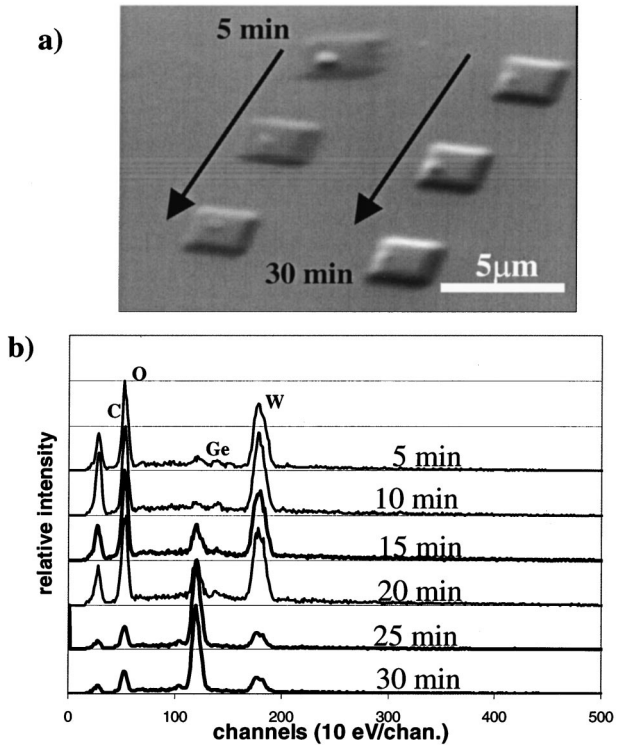

FIG. 1. (a) EDS spectra and (b) electron micrograph of electron-beam-stimulated deposition of $W(CO)_6$ at 5, 10, 15, 20, 25, and 30 min.

carbon nanopillars grown from hydrocarbon sources and a 150 nm selectively etched tungsten film.

A significant effort has been directed toward the selective electron-beam etching of technologically important materials. Thus far, we have focused on fluorine-based etch chemistries such as SF_6 and XeF_2 and have etched Si, SiO_2, Si_3N_4, Ta, Al, Cr, C, TaN, Cu, low dielectric materials, and photoresist. Figure 3 shows an electron-beam-stimulated etch of a SiO_2/Si stack that was etched with XeF_2 gas at a total background pressure of 0.1 Pa. The localized gas pressure at the substrate is likely an order of magnitude greater than the average chamber pressure because of the close proximity of the expansion nozzle to the substrate ($\sim$1 cm).

The lateral dimension of the etched feature shown in Fig. 3 is $\sim$620 nm and the vertical depth is 950 nm. The electron beam was scanned over a square region with a 0.25 μm box edge during the etching process. The diameter of the scanning electron beam in vacuum was $\sim$50 nm. Secondary electrons emerge from the sample a maximum distance of 5λ from the beam center where λ is the electron inelastic mean-free path in the specimen. Typical values of λ are $\sim$1 nm so the total beam interaction diameter should theoretically be $\sim$60 nm. The etched feature shown in Fig. 3 has a radial damage pattern 185 nm larger than the prescribed box size which is $\sim$3 times greater than the beam interaction diameter. The discrepancy is believed to be due to primary beam scattering by the XeF_2 gas.

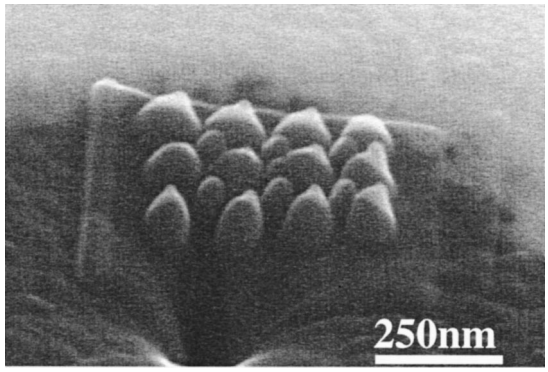

FIG. 2. Scanning electron micrograph of an array of 55 and 85 nm carbon nanopillars nearby a 150 nm etched tungsten film.

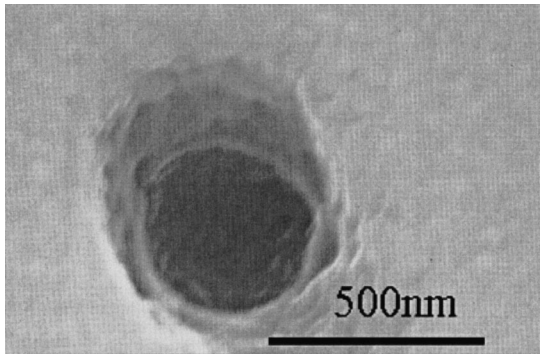

FIG. 3. Scanning electron micrograph of an electron-beam-stimulated etch of an SiO_2/Si stack.

Monte Carlo simulation of elastic electron-gas scattering

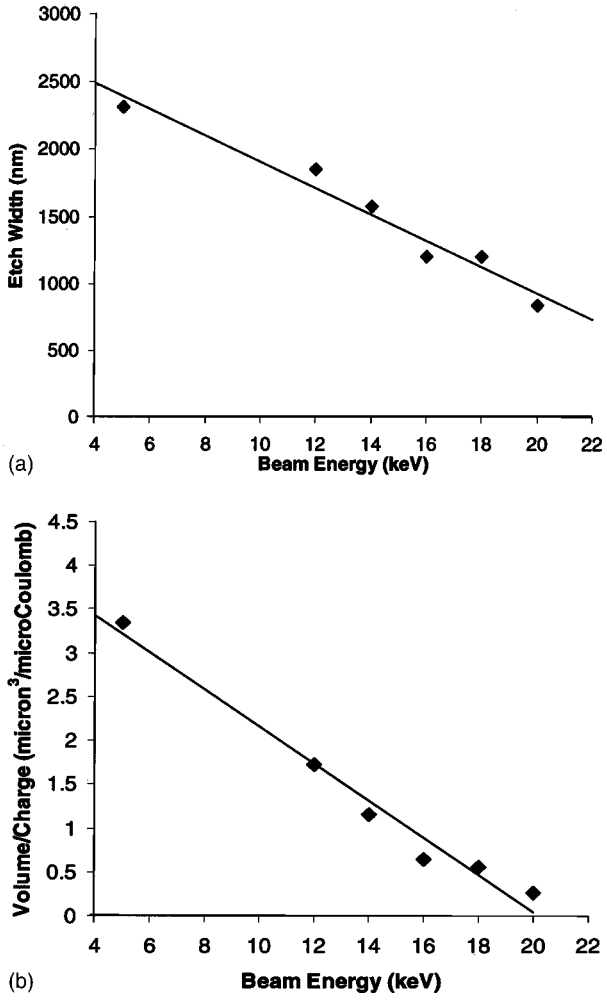

FIG. 4. (a) Plot of the silicon etch volume per Coulomb dose vs primary beam energy and (b) a plot of the etched silicon feature diameter as a function of primary beam energy.

events has been performed, however, elastic scattering angles are too large to account for the observed broadening. Inelastic scattering events with scattering angles of 10^{-3}–10^{-5} rad most likely caused the beam broadening that lead to the etch profile observed. The elastic scattering Monte Carlo simulation is being modified to include small angle inelastic scattering events to better quantify the spatial distribution of electron flux at the substrate surface.

A series of experiments were performed to elucidate the effect of incident beam energy on etch rate and damage geometry. In this instance, the electron beam was scanning during etching over a 0.25 μm$\times$0.25 μm square region and the beam current used was $\sim$1 nA. Figure 4(a) shows a plot of the silicon etch volume/Coulomb dose as a function of beam energy with the associated linear regression fit of the data ($R^2=95\%$), which shows a linear trend of increased etch rates at lower beam energies. This trend is indicative of the expected increase in the inelastic dissociation and ionization at lower beam energies. However, it is not conclusive whether the primary electrons or the secondary electrons are the dominant contributor to XeF_2 dissociation. Several groups have observed higher electron-stimulated deposition rates at lower energy and have suggested that the rate increase is due to a higher secondary electron yield at lower energy. An integration of the secondary electron energy distribution from silicon at 3 keV (with a total yield of $\delta=0.37$) and an ionization cross section of SF_6 reveals that the ratio of ionization events caused by the primary beam relative to the secondary electrons is $\sim$2.5/1. A more-detailed analysis including dissociation reactions is needed to fully account for the all of the species (ions and radicals) that are participating in the etching reaction. Figure 4(b) is a plot of the etched feature diameter and the associated linear regression fit of the data ($R^2=98\%$) and reveals that the effective spot size increased with decreasing beam energy. This trend agrees with speculation that inelastic gas scattering is occurring, as most inelastic cross sections are strong functions of energy and decrease with increasing electron energy.

[1] Y. Darici, P. H. Holloway, J. Sebastian, T. Trottier, S. Jones, and J. Rodriquez, J. Vac. Sci. Technol. A **17**, 692 (1999).
[2] R. R. Kunz and T. M. Mayer, J. Vac. Sci. Technol. B **6**, 1557 (1988).
[3] K. L. Lee and M. Hatzakis, J. Vac. Sci. Technol. **7**, 1941 (1989).
[4] I. Utke, P. Hoffmann, B. Dwir, K. Leifer, E. Kapon, and P. Doppelt, J. Vac. Sci. Technol. B **18**, 3168 (2000).
[5] A. Folch, J. Tejada, C. H. Peters, and M. S. Wrighton, Appl. Phys. Lett. **66**, 2080 (1995).
[6] R. R. Kunz, T. E. Allen, and T. M. Mayer, J. Vac. Sci. Technol. B **5**, 1427 (1987).
[7] R. R. Kunz and T. M. Mayer, Appl. Phys. Lett. **50**, 962 (1987).
[8] S. Matsui and M. Mito, Appl. Phys. Lett. **53**, 1492 (1988).
[9] S. Lipp, L. Frey, C. Lehrer, B. Frank, E. Demm, S. Pauthner, and H. Ryssel, J. Vac. Sci. Technol. B **14**, 3920 (1996).
[10] T. J. Stark, T. M. Mayer, D. P. Griffis, and P. E. Russel, J. Vac. Sci. Technol. B **10**, 2685 (1992).
[11] O. Yavas, C. Ochiai, M. Takai, A. Hosono, and S. Okuda, Appl. Phys. Lett. **76**, 3319 (2000).
[12] M. Takai, T. Kishimoto, H. Morimoto, Y. K. Park, S. Lipp, C. Lehrer, L. Frey, H. Ryssel, A. Hosono, and S. Kawabuchi, Microelectron. Eng. **41/42**, 453 (1998).
[13] P. C. Hoyle, J. R. A. Cleaver, and H. Ahmed, Appl. Phys. Lett. **64**, 1448 (1994).
[14] H. W. P. Koops, R. Weiel, D. P. Kern, and T. H. Baum, J. Vac. Sci. Technol. B **6**, 477 (1988).
[15] P. C. Hoyle, J. R. A. Cleaver, and H. Ahmed, J. Vac. Sci. Technol. B **14**, 662 (1996).
[16] K. T. Kohlmann-von Platen, J. Chiebek, M. Weiss, K. Reimer, H. Oertel, and W. H. Brunger, J. Vac. Sci. Technol. B **11**, 2219 (1993).
[17] R. B. Jackson and J. S. Foord, Appl. Phys. Lett. **49**, 196 (1986).
[18] M. Komuro and H. Hiroshima, Microelectron. Eng. **35**, 273 (1997).
[19] N. A. Kislov, I. I. Khodos, E. D. Ivanov, and J. Barthel, Scanning **18**, 114 (1996).
[20] K. T. Kohlmann, M. Thiemann, and W. H. Brunger, Microelectron. Eng. **13**, 279 (1991).
[21] S. Matsui and K. Mori, J. Vac. Sci. Technol. B **4**, 299 (1986).
[22] K. T. Kohlmann-von Platen and W. H. Brunger, J. Vac. Sci. Technol. B **14**, 4262 (1996).
[23] S. Matsui, T. Ichihashi, and M. Mito, J. Vac. Sci. Technol. **7**, 1182 (1989); R. R. Kunz and T. M. Mayer, J. Vac. Sci. Technol. B **5**, 427 (1987).
[24] J. W. Coburn and H. F. Winters, J. Appl. Phys. **50**, 3189 (1979).
[25] P. E. Russell (private communications).